Magnetic phase diagram and electronic structure of UPt_2Si_2 at high magnetic fields: A possible field-induced Lifshitz transition

D. Schulze Grachtrup,[1] N. Steinki,[1] S. Süllow,[1] Z. Cakir,[2] G. Zwicknagl,[2] Y. Krupko,[3] I. Sheikin,[3] M. Jaime,[4] and J. A. Mydosh[5]

[1]*Institut für Physik der Kondensierten Materie, TU Braunschweig, D-38106 Braunschweig, Germany*

[2]*Institut für Mathematische Physik, TU Braunschweig, D-38106 Braunschweig, Germany*

[3]*Laboratoire National des Champs Magnétiques Intenses (LNCMI-EMFL), CNRS, UGA, 38042 Grenoble, France*

[4]*National High Magnetic Field Laboratory, Los Alamos National Laboratory, Los Alamos, New Mexico 87545, USA*

[5]*Kamerlingh Onnes Laboratory and Institute Lorentz, Leiden University, 2300RA Leiden, Netherlands*

(Received 8 November 2016; revised manuscript received 30 January 2017; published 14 April 2017)

We have measured the Hall effect, magnetotransport, and magnetostriction on the field-induced phases of single-crystalline UPt_2Si_2 in magnetic fields up to 60 T at temperatures down to 50 mK, firmly establishing the phase diagram for magnetic fields $B\|a$ and c axes. Moreover, for the $B\|c$ axis we observe strong changes in the Hall effect at the phase boundaries. From a comparison to band structure calculations utilizing the concept of a dual nature of the uranium $5f$ electrons, we propose that these represent field-induced topological changes of the Fermi surface due to at least one Lifshitz transition. Furthermore, we find a unique history dependence of the magnetotransport and magnetostriction data, indicating that the proposed Lifshitz-type transition is of a discontinuous nature, as predicted for interacting electron systems.

DOI: 10.1103/PhysRevB.95.134422

I. INTRODUCTION

Lifshitz transitions, that is, quantum phase transitions involving topological changes of the Fermi surface and thus referred to as electronic topological transitions (ETTs), have been proposed to play a major role in the physics of correlated electron systems. Here, a variety of exotic field-induced phases, as well as unconventional pressure-induced phases (including unconventional superconducting ones), has been observed and attributed to Lifshitz transitions [1–11].

The theory of ETTs was developed to account for the ground-state properties of certain materials under wide variation of external parameters such as pressure [12,13]. It considered noninteracting electrons at zero temperature, yielding a continuous transition of 2.5 orders, which reflects the exponent in the Ehrenfest expression in three dimensions. Later, based on various experimental observations, the case of interacting electrons was treated in detail [14–18]. Here, conceptually, a (low) energy scale is associated with the interacting electron system, which may produce ETTs in experimentally accessible magnetic field and pressure ranges of a few tens of teslas and gigapascals. Also, it was predicted that for interacting electron systems the transitions inherently become discontinuous [14,15].

Regarding the experimental verification of electronic topological transitions, cases of real materials exhibiting Lifshitz transitions are rare. On general grounds, it has been demonstrated that anomalies from ETTs should be observable in various transport properties [13,19]. Yet ETTs exist only for zero temperature and smear out with finite temperature. It is a formidable experimental task to identify a Lifshitz-type transition, requiring experiments down to low temperatures under extreme conditions. Also, for correlated electron systems, calculating the band structure as a function of external control parameters is a very challenging task.

A case in point is the intermetallic $5f$ electron system UPt_2Si_2. The material belongs to the large class of UT_2M_2 compounds (T = transition metal, M = Si or Ge) and crystallizes in the tetragonal $CaBe_2Ge_2$ structure (space group P4/*nmm*) [20]. In zero magnetic field, it undergoes an antiferromagnetic (AFM) transition at $T_N = 32$ K. The magnetic structure consists of moments $\mu_{\rm ord} \sim 2.5\mu_B$ ferromagnetically aligned within the ab plane and antiferromagnetically coupled and pointing along the c axis [21,22]. The simple magnetic structure with a large magnetic moment, combined with a moderately enhanced electronic contribution to the specific heat $\gamma = 32\,\mathrm{mJ/mol\,K^2}$, was taken as the indicator for UPt_2Si_2 to be one of the rare examples of a uranium intermetallic local moment magnet. Correspondingly, a crystal electric field (CEF) scheme for the $5f^2$ state of the uranium ion was proposed that has been used to explain initial high-field magnetization measurements and the anisotropy of the susceptibility [23,24]. Additional fine structure in the magnetization observable in the field range ∼20−40 T was not considered to be at odds with the CEF concept.

Based on an extensive reinvestigation of the magnetization, we have demonstrated that the agreement between the CEF model and experimental data does not hold up at high fields. For magnetic fields $B \parallel a$ axis, aside from the suppression of AFM order, there is a hysteretic high-field (∼40 T) regime whose nature is not understood as yet [25,26] (see Fig. 7 below). Moreover, for fields $B \parallel c$ axis, above 24 T the experimental data strongly deviate from the CEF theoretical predictions. In particular, a complex series of field-induced phases is observed above 24 T which cannot be attributed only to spin reorientation processes and/or crystal-field effects [23–26]. As an alternative to the CEF model, we have proposed that an itinerant picture of the properties of UPt_2Si_2 is more appropriate, a view supported by recent band structure calculations [27]. Moreover, these calculations have highlighted the relevance of correlation effects in this system [27,28]. Also, the general character of the band structure has been revealed to be "quasi-two-dimensional" as a result of the comparatively low crystallographic symmetry. This two-dimensional character is

reflected, for instance, in the highly anisotropic resistivity of UPt_2Si_2 [22].

In Ref. [25], we have argued that the observation of the field-induced phases in UPt_2Si_2 is related to Lifshitz-type transitions. To test the validity of this concept in UPt_2Si_2, studies at the lowest temperatures using experimental tools directly testing the Fermi surface (FS) and the order of the phase transitions are required. A test of the FS by means of quantum oscillation measurements cannot be performed for UPt_2Si_2, as the oscillations are suppressed by intrinsic structural disorder from strained Pt(2)/Si(2) layers in the $CaBe_2Ge_2$ lattice [22]. Therefore, more integral, and less disorder dependent, probes of the FS need to be investigated to check the Lifshitz scenario for UPt_2Si_2. In addition, to establish the order of the field-induced phase transitions experimental probes sensitive to the structural properties may be used. If combined with band structure calculations, an assessment of the nature of the field induced phases in UPt_2Si_2 may be possible.

In this situation, we present a study on UPt_2Si_2 under extreme conditions, that is, at temperatures down to 50 mK and in fields up to 60 T, using the Hall effect, magnetotransport, and magnetostriction. Our experiments clearly demonstrate changes of the FS in high magnetic fields. Our study is complemented by band structure calculations utilizing the concept of the dual nature of the uranium $5f$ electrons which simulate the effect of magnetic fields on the topology of the band structure. As a result of these calculations, it is verified that Lifshitz-type transitions may be induced in high magnetic fields in UPt_2Si_2.

II. EXPERIMENTAL DETAILS

The experiments presented here were performed on single-crystalline UPt_2Si_2, with the samples being as cast and bar shaped with a cross section $\sim 1\times 1\,\mathrm{mm}^2$ and a length of a few millimeters. The material from the same single crystal was characterized in Refs. [22,25,26,29].

The electronic transport studies were carried out at the Laboratoire National des Champs Magnétiques Intenses in dc fields up to 34 T directed along the a and c axes. For the experiments inside the magnet bore a dilution cryostat was installed. Data were taken with a standard lock-in setup, with a reasonable signal-to-noise ratio obtained with a measurement current of 1 mA directed along the a axis. This resulted in an equilibrium temperature of 120 mK, with additional experiments with lower currents carried out down to 50 mK. Accordingly, we now have access to a wide range of the field/temperature plane up to a B/T ratio of almost 700 T/K.

The sample was fitted onto a rotatable sample holder and immersed into the helium mixture. Up to ten electrical contacts were glued on the sample surfaces with silver paint to allow for simultaneous measurements of transverse magnetoresistivity and the Hall effect for each magnetic field direction. In a second round of experiments, the same setup was used, but now to measure the longitudinal magnetoresistivity. Finally, axial magnetostriction experiments were performed at the Los Alamos High Field Laboratory in pulsed fields up to 60 T directed along the a and c axes. Here, the base temperature was 1.4 K, with the experiment performed using an optical fiber with a Bragg grating [30,31].

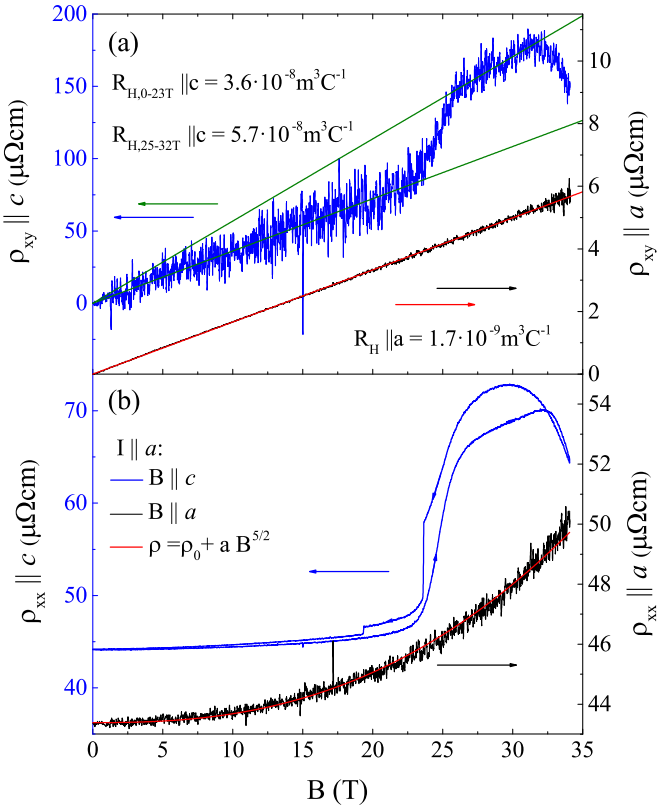

FIG. 1. Comparative plot of (a) Hall resistivity ρ_{xy} at $T = 300$ mK for $B \parallel a$ and 130 mK for $B \parallel c$ axis together with fits to the data and (b) transverse magnetoresistivity of UPt_2Si_2 at $T = 300$ mK for $B \parallel a$ and 120 mK for $B \parallel c$. For details see the text.

III. RESULTS

For fields $B \parallel a$ axis up to 34 T and low T, the Hall resistivity ρ_{xy} is linear in B [Fig. 1(a)]. Consistent with Ref. [25], there are no phase transitions in this field range. Next, the Hall effect data for $B \parallel c$ axis up to 34 T are included in Fig. 1(a), and the full set of (low-temperature) data is summarized in Fig. 2. For fields up to 23 T, viz., in AFM phase I, ρ_{xy} increases linearly with field [25]. At the phase boundary I-III there is a distinct upward curvature in $\rho_{xy}(B)$ which becomes linear in field again in phase III. At the phase III-V boundary there is a now downwards curvature in ρ_{xy}. Within experimental scatter, no hysteresis is observed between field-sweep-up and -down measurements, and there is no temperature dependence in the range below 2 K. Qualitatively, this behavior is reminiscent of that of Rh-doped URu_2Si_2 [32].

For parametrization, the Hall effect is fitted using the expression $\rho_{xy} = R_H B$. For $B \parallel a$ axis the data in phase I yield a Hall coefficient $R_H = 1.7\times 10^{-9}\,\mathrm{m}^3/\mathrm{C}$ [solid line in Fig. 1(a)]. Correspondingly, for $B \parallel c$ axis the linear regimes from 0 to 23 and 25 to 32 T lead to Hall coefficients $R_H = 3.6\times 10^{-8}\,\mathrm{m}^3/\mathrm{C}$ and $R_H = 5.7\times 10^{-8}\,\mathrm{m}^3/\mathrm{C}$, respectively. Overall, these values are broadly consistent with the typical behavior of heavy-fermion intermetallics. We note that, although for $B \parallel c$ axis at the highest fields (34 T) the system resides in phase V (as proven by the observation of hysteresis in the magnetoresistivity; see below), in the Hall effect we observe nonmonotonic behavior in this field range.

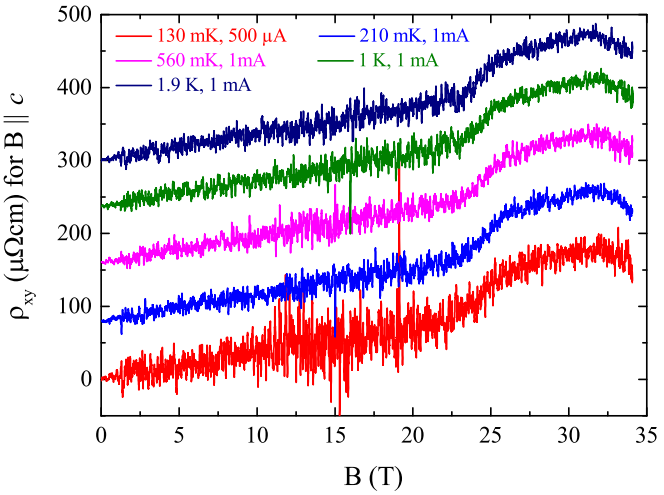

FIG. 2. Hall resistivity ρ_{xy} at various temperatures for $B \parallel c$ axis. Data are shifted for clarity. For details see the text.

The reason for the unusual behavior is not clear and will require experiments at still higher fields to solve.

In magnetic materials, the Hall effect contains two terms. The *normal* contribution $\rho_{xy}^{\text{nor}} = R_N B$ measures the carrier density n in units of the electron charge e: $R_N = (ne)^{-1}$. The *anomalous* Hall contribution ρ_{xy}^{ano} reflects terms dependent on the resistivity and/or magnetization (reported in Refs. [24–26]). Therefore, adding to the data published in Ref. [25], low-temperature magnetoresistivity has been carried out [Figs. 1(b) and 3]. At the lowest temperatures for $B \parallel a$ axis up to 34 T, for the magnetoresistivity we find to good approximation $\rho_{xx}(B) = \rho_{xx}(B = 0) + aB^{\frac{5}{2}}$. In accordance with the Hall effect and Ref. [25], we find no evidence for phase transitions.

In contrast, for $B \parallel c$ axis the transitions from phase I into III and III into V are reflected by distinct anomalies in the magnetoresistivity. The transition I $\rightarrow$ III is accompanied by a steep increase of the magnetoresistivity, with the midpoint of the upturn close to the transition field determined from

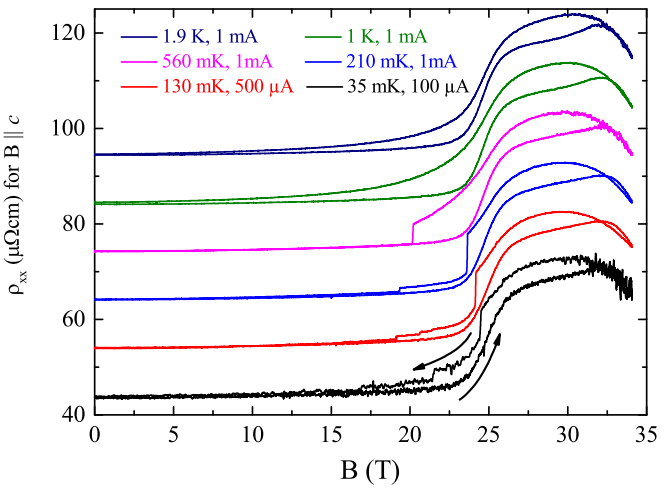

FIG. 3. Transverse magnetoresistivity of UPt_2Si_2 at various temperatures for $B \parallel c$ axis. For details see the text.

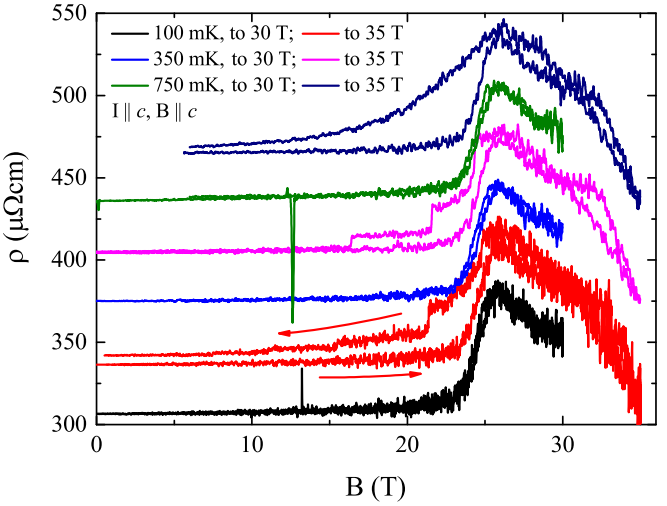

FIG. 4. Longitudinal magnetoresistivity of UPt_2Si_2 at various temperatures for $B \parallel c$ axis for field sweeps either into phase III (30 T) and back to zero field or into phase V (35 T) and back.

magnetization. Conversely, the transition III $\rightarrow$ V shows up as a corresponding drop of the magnetoresistivity.

Surprisingly, the magnetoresistivity $B \parallel c$ axis is accompanied by a curious type of hysteresis [Figs. 1(b), 3, and 4]: Measurements of $\rho_{xx}(B)$ by sweeping from zero field into phase V and back produce hysteresis in the magnetoresistivity. In contrast, sweeps from zero field only into phase III and back produce no hysteresis in $\rho_{xx}(B)$ at low T. To demonstrate this, we have carried out field-history-dependent longitudinal magnetoresistivity measurements ($B \parallel c \parallel I$) at low temperatures, which we summarize in Fig. 4. Here, we have first swept the field from zero into phase III (up to 30 T) and back to zero for various temperatures below 1 K. For this measurement sequence no hysteresis is observed in the magnetoresistivity. Conversely, for field sweeps at the same temperatures up into phase V (final field: 35 T) we detect hysteresis in the magnetoresistivity in field-sweep-down vs field-sweep-up data. This observation indicates that the phase III-V boundary denotes a first-order phase transition. Moreover, this observation is consistent with our previous magnetoresistivity study [25], where we swept the field up to 28 T, i.e., into phase III, and did not observe hysteresis.

In terms of the anomalous Hall contribution ρ_{xy}^{ano}, the absence of hysteresis in the Hall effect and its presence in the magnetoresistivity (Fig. 1) implies that ρ_{xy}^{ano} is not dependent on $\rho_{xx}(B)$. Then, the upturn in ρ_{xy} at the phase I-III boundary might be attributed to the corresponding upturn in the magnetization M (see Refs. [24–26]). Conversely, at the phase III-V boundary the downturn in ρ_{xy} is clearly at odds with the upturn in M. It implies that this phase transition is accompanied by a carrier density change, which may involve a qualitative change of the Fermi surface as in an ETT.

To complement our study on UPt_2Si_2 with a structural probe, we have carried out axial magnetostriction experiments, which we depict in Fig. 5. For $B \parallel a$ axis we find a contraction of the sample for all fields. Further, a slight change of slope occurs at elevated fields, becoming hysteretic in the temperature/field range, where magnetization hysteresis is

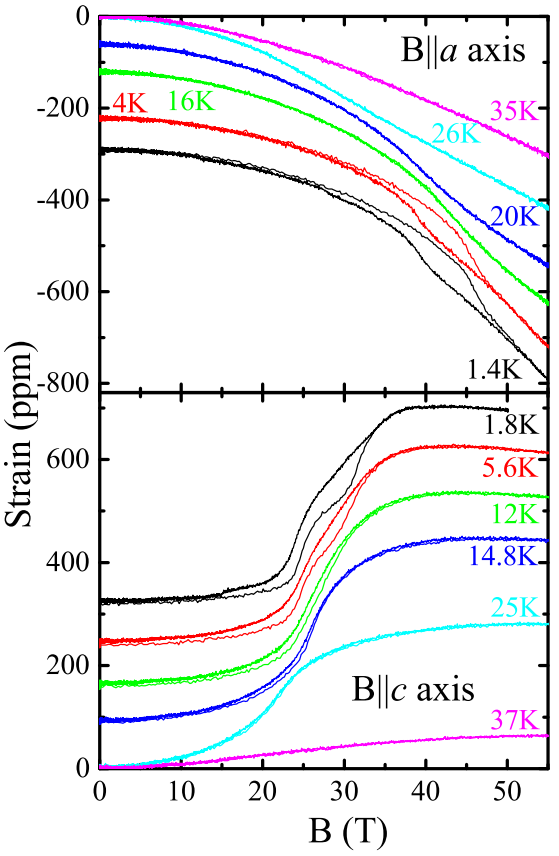

FIG. 5. Axial magnetostriction of UPt_2Si_2 for magnetic fields $B \parallel a$ and c axes plotted up to 55 T for various temperatures. Data are shifted for clarity. For details see the text.

observed. The (hysteretic) features denote the transition from phase I into the paramagnetic state.

For $B \parallel c$ axis the crystal UPt_2Si_2 expands for fields up to ∼40 T, and at the highest fields the magnetostriction saturates. The field-induced phase transitions are identified as an additional structure in the magnetostriction. Similar to the magnetization, at low temperatures there is a twofold structure in the data reflecting the transition from phase I into III and finally into phase V. The critical fields of the different phases are identified as points of maximum slope in the field-sweep-up measurements.

Like for the magnetoresistivity, we find a history-dependent hysteresis at low T (Fig. 6): For measurements from zero field up into phase III and back no hysteresis is observed. Conversely, when the final field lies within phase V, structural hysteresis appears. Thus, the structural probe magnetostriction verifies that the phase transition III-V is of a first-order nature.

With the present data set we complete our high-field studies of UPt_2Si_2. By combining the new data with those from Ref. [25], we present the magnetic phase diagrams of UPt_2Si_2 for $B \parallel a$ and c axes in Fig. 7. Altogether, our new set of data fully confirms the essential findings on the magnetic phase diagrams of UPt_2Si_2 as reported in Ref. [25]. In particular, for the field $B \parallel a$ axis, the new data points derived from magnetostriction measurements, which define the phase border lines from the AFM phase I into the hysteretic regime II and the paramagnetic regime, sit well

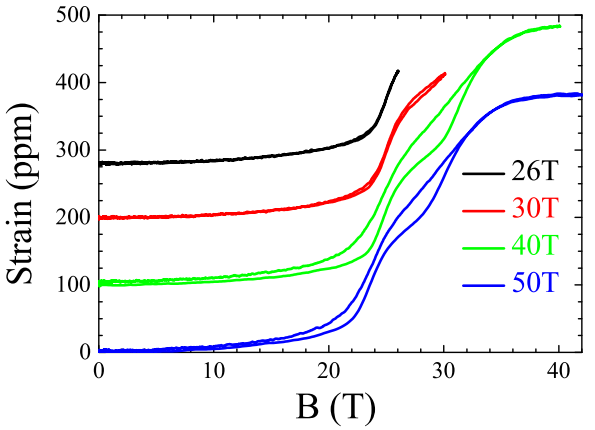

FIG. 6. Axial magnetostriction of UPt_2Si_2 for magnetic fields $B \parallel c$ axis at 1.8 K. Data are shifted for clarity. The plot illustrates the absence and appearance of structural hysteresis upon ramping the field into phases III and V, respectively. The legend denotes the highest magnetic fields attained for the different magnet runs; for details see the text.

on top of those previously established. Furthermore, in the intermediate-temperature regime ∼20 – 30 K the new data now define the border lines more accurately than was possible with the data presented in Ref. [25].

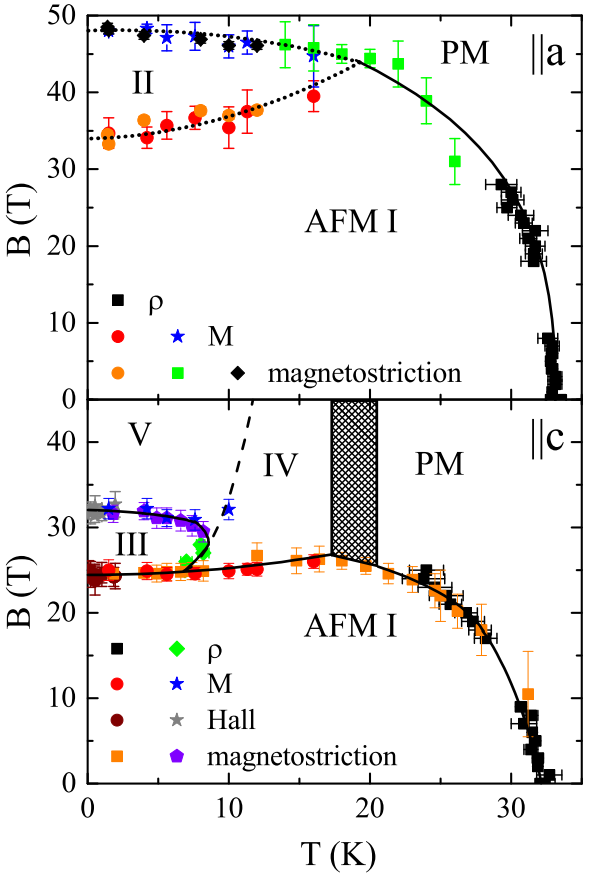

FIG. 7. The magnetic phase diagrams of UPt_2Si_2 for the field $B \parallel a$ and c axes from combining the present data with those reported in Ref. [25]. For details see the text.

For the field $B \parallel c$ axis at low temperatures the border lines between phases I, III, and V are perfectly reproduced with our new data. Furthermore, the existence and nature of the phase border lines have been established down into the millikelvin range. Finally, with the new data the phase border lines are now more accurately determined in the intermediate-temperature regime $\sim 15 - 25$ K.

As we have noted before [25], we believe that there must be additional phase border lines in high magnetic fields between the paramagnetic regime and phase IV and between phase IV and III/V. These observations are based on the qualitative change in the field-dependent character of the magnetization (see Fig. 1 with field $B \parallel c$ axis in Ref. [25]). First, the magnetization at 20 K and above evolves monotonically in a Brillouin-function-like fashion with field, while for the data taken at 16 K and below there is a hysteretic metamagnetic transition at around 25 T. Therefore, the metamagnetic transition must be into a phase different from the paramagnetic regime, viz., into phase IV. Also, the magnetization taken in the temperature range $\sim$10 to 16 K exhibits a single metamagnetic transition, while for data at 10 K and below there is a two-step transition (the same has been observed in the magnetostriction; see above). Following a similar line of argumentations, we have concluded that a transition into a new phase V occurs at low temperatures.

From our previous data we could only roughly estimate the position of these phase border lines and the associated tricritical points. With our magnetostriction data we can more accurately define the evolution of the phase border lines, as done in Fig. 7. Notably, the new data suggest that for $B \parallel c$ axis the border line of phase I exhibits a shallow maximum around $\sim$20 K/25 T. Such behavior would be highly unusual for a common antiferromagnet. Instead, it appears that the competition with the high-field phase IV produces this anomalous evolution of the phase border line. Hence, our new data are fully consistent with the phase diagram scenario labeled "A" in Ref. [25]. Within this scenario, we conclude that the upper tricritical point lies at around 25 T and 19 K. Unfortunately, close inspection of our various data sets utilizing different experimental tools does not provide a clear-cut signature unambiguously defining the tricritical point. Also, the precise evolution of the border between phases IV and V is rather awkward, as is the detailed structure of the area around the tricritical phase III-IV-V point. Ultimately, to unambiguously establish and define these phase border lines and to definitely discard scenario B from Ref. [25], experiments in high magnetic fields carried out as a function of temperature are still required. Unfortunately, given the high field range, such experiments are rarely carried out.

IV. BAND STRUCTURE CALCULATIONS

For $B \parallel c$ axis the experimental evidence is consistent with the transition into phase V being an ETT in a correlated electron system. We have observed a significant change in the Hall coefficient at the phase III-V transition for $B \parallel c$ axis, in line with a Lifshitz-type character. Also, the first-order nature of this transition is consistent with a Lifshitz-type transition for an interacting electron system. As the next step, to complement our experimental study, we carried out additional band structure calculations with the aim of identifying features in the band structure beyond those established in Ref. [27].

For an ETT, the topological changes in the isoenergy surfaces result from critical points in the band dispersion, i.e., minima, saddle points, and maxima, which give rise to Van Hove singularities in the density of states. The changes in the topology of the isoenergy surfaces include the appearance or disappearance of small pockets, the formation of voids, and the disruption of necks. Therefore, the focus of the present calculations is on critical points in the quasiparticle dispersion of UPt_2Si_2. For magnetic-field-induced Lifshitz transitions, the critical points have to be rather close to the Fermi energy. All in all, it is thus the occurrence of these pockets, voids, or necks that we are searching for in the band structure.

The present calculations assume that there are itinerant $5f$ electrons which form partially filled coherent bands. We analyze the Fermi surface where the energy bands are calculated under the following assumptions about the nature of the $5f$ electrons: We begin by adopting density-functional theory treating all $5f$ electrons as band states. This approximation scheme cannot fully capture the correlation effects. To simulate the latter we calculate the band structure under the assumption that two of the $5f$ electrons are localized while one may be itinerant and hybridize with the conduction states. For simplicity, we first treat all $5f$ channels as equivalent and account for orbital selection in the second step. For the last step, we single out the $5f$ electron in the $j = 5/2$, $j_z = \pm 1/2$ channel as the hybridized electron.

More specifically, the band structure results reported in the present paper were obtained with the fully relativistic formulation of the linear muffin-tin orbital (LMTO) method [33–36]. The spin-orbit interaction is fully taken into account by solving the Dirac equation. The results are compared to the relativistic calculations by Elgazzar *et al.* [27]. Because the heavy-fermion compound UPt_2Si_2 crystallizes in the tetragonal $CaBe_2Ge_2$ structure, the crystal structure is relatively open, and,consequently, the atomic-sphere approximation (ASA) cannot be expected to give a sufficiently accurate description of the electronic band structure. The combined correction term which contains the leading corrections to the ASA alters [33] the conduction bands in a characteristic way and hence cannot be neglected. Exchange and correlation effects were introduced using the Barth-Hedin potential [37]. The band structure was converged for 405 **k** points in the irreducible wedge, whose volume equals 1/16 of the Brillouin zone. The density of states (DOS) was evaluated using the tetrahedron method with linear interpolation for the energies [38,39]. For the conduction band the DOS was calculated at 0.25 mRy ($\approx$0.0034 eV) intervals.

The effective potential seen by the conduction states is approximately constructed as a superposition of contributions which have spherical symmetry inside atomic spheres and "empty" spheres surrounding lattice or interstitial sites, respectively. The empty spheres should be viewed as auxiliary constructions that permit an improved description of the electron density as well as the potential within the framework of the ASA. In UPt_2Si_2 the dominant contribution to the charge in the interstitial region comes from the Pt d states.

Our calculations are done with the experimental lattice parameters and do not correspond to the equilibrium geometry

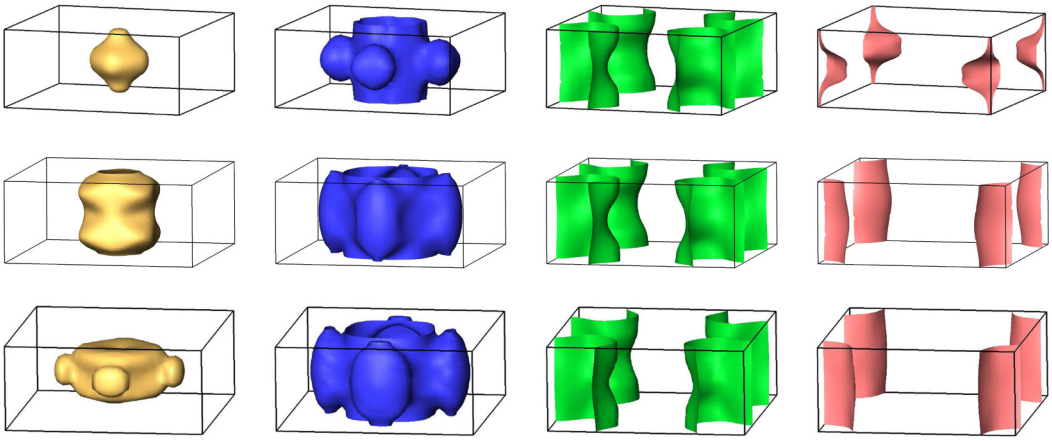

FIG. 8. Calculated Fermi surfaces of UPt_2Si_2 in the paramagnetic phase. Top: LDA calculation treating all $5f$ electrons as itinerant band electrons. Middle: Two $5f$ electrons are treated as part of the ion core while one $5f$ electron hybridizes with the conduction electrons. Bottom: Influence of orbital-selective localization is accounted for by treating two $5f$ electrons as part of the ion core while one $5f$ electron in the $j = 5/2$, $j_z = \pm 1/2$ channel hybridizes with the conduction electrons.

of an local-density approximation (LDA) calculation. The total energy evaluated for the experimental structure will therefore exceed its theoretical minimum value. This difficulty, which is generally encountered in metals with strongly correlated electrons, is a direct consequence of the LDA description of these systems in terms of a single-particle picture. This can be seen by considering two limiting cases. First, treating the f electrons as part of the ion core implies that their contribution to binding is neglected. As a consequence, the equilibrium values of the lattice constants are often overestimated. Second, describing the f electrons as band electrons yields a relatively narrow, partially filled f band at the Fermi level. The calculated LDA DOS at the Fermi level is large compared with that of ordinary metals. An effective single-particle description such as the LDA predicts an electronic compressibility which is enhanced over that of ordinary metals by the same factor. The behavior anticipated for independent fermions, however, is in contradiction to experiment, which yields compressibility values for heavy-fermion metals which are comparable to those of ordinary metals. The large electronic compressibility predicted erroneously by the LDA in f metals leads to overbinding (i.e., the theoretical values of the equilibrium lattice constants are too small). It is a direct consequence of the failure of the independent particle picture.

The calculations were done using two energy panels; that is, two separate LMTO calculations were performed to determine self-consistently the uranium $6p$ states and the conduction bands, respectively. Treating the U $6p$ semicore states as band states accounts for the small overlap between these core states. The resulting narrow bands far below the Fermi energy hybridize only weakly with the conduction bands. This hybridization is then neglected in our method, but its influence on the shape of the potential is taken into account. The charge contributions of the other core states were taken from atomic calculations and kept frozen during the iterative procedure. For the lower panel we included $s-p-d$ angular momentum components in the basis at the U and Pt sites and $s-p$ components at the Si and interstitial sites. For the upper panel we included $s-p-d-f$ components at the U site and $s-p-d$ in the remaining sites.

The Fermi surfaces obtained with the three approaches regarding the degree of localization of the $5f$ electrons are summarized in Fig. 8. We find four bands crossing the Fermi energy and denote the corresponding FS sheets as 1, 2, 3, and 4. Globally, the LDA result agrees well with the one obtained by Elgazzar *et al.* [27] apart from the fact that the "appendices" are absent in our sheet 1 (see Elgazzar band labeled 113).

With respect to the FS topology, we find that FS sheets 3 and 4 are remarkably insensitive to the treatment of the $5f$ states. The number of itinerant $5f$ electrons affects only sheets 1 and 2. Correspondingly, we have inspected closely the response of these sheets on magnetic field by analyzing the isoenergy surfaces for shifts away from the Fermi energy by 6 meV. For a magnetic moment $\sim 2.5\mu_B$ as in UPt_2Si_2 this value corresponds to a magnetic field of ~ 30 T.

In particular, for sheet 2 we find a qualitative change in the shape of the FS for such a small energy shift, thus providing direct band structure evidence for an ETT (see Fig. 9). Clearly, a void formation/neck disruption is visible as the isoenergy surface is tuned from -6 to $+6$ meV around the Fermi energy. For FS sheet 1 in the energy range considered we find no topological change.

Following the identification of Fermi surface sheet 2 as the one being topologically affected by magnetic fields of the

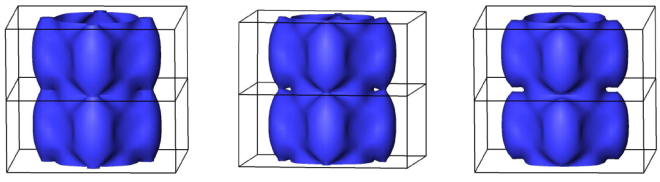

FIG. 9. Lifshitz transitions for the case of two $5f$ electrons treated as localized. The isoenergy surfaces $E = E_F - 6$ meV (left), $E = E_F$ (middle), and $E = E_F + 6$ meV (right) show a cascade of ETTs by void formation and neck disruption which are accessible by magnetic fields in the range of a few tens of teslas.

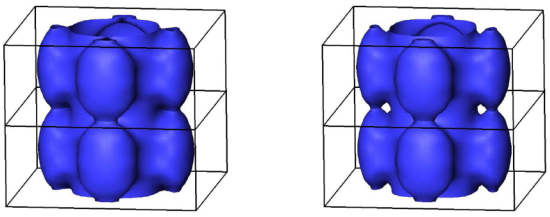

FIG. 10. ETTs in the dual model treating two $5f$ electrons as localized and allowing the $5f$ ($j = 5/2$, $j_z = \pm 1/2$) channel to hybridize with the conduction bands. Depicted are the isoenergy surfaces $E = E_F - 6$ meV (left) and $E = E_F + 6$ meV (right).

order of 30 T, in the final step we have specified the character of the itinerant electron by allowing the $5f$ ($j = 5/2$, $j_z = \pm 1/2$) channel to hybridize with the conduction bands. Again, the isoenergy surfaces shifted by ± 6 meV against the Fermi energy clearly reflect an ETT, as demonstrated in Fig. 10. Thus, in our band structure calculations, assuming one out of three $5f$ electrons being delocalized, we find ETTs on the Fermi surfaces of a correlated electron system, viz., UPt_2Si_2, consistent with our experiments.

V. CONCLUSION

In summary, we provided experimental evidence of the possibility of a field-induced first-order Lifshitz-type transition in the correlated electron system UPt_2Si_2 through a combined study of the electronic and structural properties. Furthermore, for the FS, critical points close to the Fermi energy E_F were found in the band dispersion when two of the $5f$ electrons were treated as localized, implying that field-induced Lifshitz transitions are to be expected. In contrast, for the all-itinerant model, the critical points leading to Lifshitz transitions are too far from the Fermi energy to be relevant in an experimental context. Thus, with our study we demonstrated the consistence of our experiments with the predictions made based on the dual model of $5f$ electrons for the case of a uranium intermetallic with strong electronic correlations.

Finally, a question arises about the nature of the other magnetic phases in UPt_2Si_2 for $B \parallel c$ axis. When associating the first-order transition into phase V with an ETT, oppositely, the second-order character of the phase I-III transition would signal a more ordinary type of transition. The character of the transition, as seen in the magnetization (see Ref. [25]), together with the size of the jump of the magnetization, could be consistent with, for instance, a spin-flop transition. In turn, this observation raises questions about the character of phase IV, as it shows up in the magnetization in a fashion similar to the I-III transition. In terms of the magnetization, the difference between phases III and IV is not obvious.

Conversely, following a different line of arguments, while thermal smearing might prohibit a definite identification, conceptually, phase IV can have the FS topology of phase I/III, phase V, or a different one. If the FS topology were not that of phases I/III, consequently, there would be multiple Lifshitz transitions in the phase diagram for $B \parallel c$ axis of UPt_2Si_2. Taking this observation into a more general context, the interplay of spin reorientation/anisotropy and FS topology may give rise to a complex set of field-induced phases in UPt_2Si_2, which might be relevant to related exotic phenomena such as the complex phase diagram of URu_2Si_2 [32,40,41].

ACKNOWLEDGMENTS

We acknowledge the support of the LNCMI-CNRS, a member of the European Magnetic Field Laboratory (EMFL). We gratefully acknowledge support from the Braunschweig International Graduate School of Metrology B-IGSM and the DFG Research Training Group GrK1952/1 Metrology for Complex Nanosystems. Work at the National High Magnetic Field Laboratory was supported by National Science Foundation Cooperative Agreement No. DMR-1157490 and the state of Florida, as well as the Strongly Correlated Magnets thrust of the U.S. Department of Energy, Basic Energy Sciences, Science in 100T program.

[1] N. Kozlova, J. Hagel, M. Doerr, J. Wosnitza, D. Eckert, K.-H. Müller, L. Schultz, I. Opahle, S. Elgazzar, M. Richter, G. Goll, H. v. Löhneysen, G. Zwicknagl, T. Yoshino, and T. Takabatake, Phys. Rev. Lett. **95**, 086403 (2005).

[2] P. M. C. Rourke, A. McCollam, G. Lapertot, G. Knebel, J. Flouquet, and S. R. Julian, Phys. Rev. Lett. **101**, 237205 (2008).

[3] T. Plackowski, D. Kaczorowski, and J. Sznajd, Phys. Rev. B **83**, 174443 (2011).

[4] E. A. Yelland, J. M. Barraclough, W. Wang, K. V. Kamenev, and A. D. Huxley, Nat. Phys. **7**, 890 (2011).

[5] M. Deppe, S. Lausberg, F. Weickert, M. Brando, Y. Skourski, N. Caroca-Canales, C. Geibel, and F. Steglich, Phys. Rev. B **85**, 060401 (2012).

[6] H. Pfau, R. Daou, S. Lausberg, H. R. Naren, M. Brando, S. Friedemann, S. Wirth, T. Westerkamp, U. Stockert, P. Gegenwart, C. Krellner, C. Geibel, G. Zwicknagl, and F. Steglich, Phys. Rev. Lett. **110**, 256403 (2013).

[7] A. Pourret, G. Knebel, T. D. Matsuda, G. Lapertot, and J. Flouquet, J. Phys. Soc. Jpn. **82**, 053704 (2013).

[8] H. R. Naren, S. Friedemann, G. Zwicknagl, C. Krellner, C. Geibel, F. Steglich, and S. Wirth, New J. Phys. **15**, 093032 (2013).

[9] D. Aoki, G. Knebel, and J. Flouquet, J. Phys. Soc. Jpn. **83**, 094719 (2014).

[10] D. Aoki, G. Seyfarth, A. Pourret, A. Gourgout, A. McCollam, J. A. N. Bruin, Y. Krupko, and I. Sheikin, Phys. Rev. Lett. **116**, 037202 (2016).

[11] G. Bastien, A. Gourgout, D. Aoki, A. Pourret, I. Sheikin, G. Seyfarth, J. Flouquet, and G. Knebel, Phys. Rev. Lett. **117**, 206401 (2016).

[12] I. M. Lifshitz, Sov. Phys. JETP **11**, 1130 (1960).

[13] A. A. Varlamov, V. S. Egorov, and A. V. Pantsulaya, Adv. Phys. **38**, 469 (1989).

[14] Y. Yamaji, T. Misawa, and M. Imada, J. Phys. Soc. Jpn. **75**, 094719 (2006).

[15] Y. Yamaji, T. Misawa, and M. Imada, J. Magn. Magn. Mater. **310**, 838 (2007).
[16] P. Schlottmann, J. Appl. Phys. **111**, 07E101 (2012).
[17] M. Bercx and F. F. Assaad, Phys. Rev. B **86**, 075108 (2012).
[18] Y. Wang, M. N. Gastiasoro, B. M. Andersen, M. Tomic, H. O. Jeschke, R. Valenti, I. Paul, and P. J. Hirschfeld, Phys. Rev. Lett. **114**, 097003 (2015).
[19] S. G. Sharapov, V. P. Gusynin, and H. Beck, Phys. Rev. B **67**, 144509 (2003).
[20] K. Hiebl and P. Rogl, J. Nucl. Mater. **144**, 193 (1987).
[21] R. A. Steeman, E. Frikkee, S. A. M. Mentink, A. A. Menovsky, G. J. Nieuwenhuys, and J. A. Mydosh, J. Phys.: Condens. Matter **2**, 4059 (1990).
[22] S. Süllow, A. Otop, A. Loose, J. Klenke, O. Prokhnenko, R. Feyerherm, R. W. A. Hendrikx, J. A. Mydosh, and H. Amitsuka, J. Phys. Soc. Jpn. **77**, 024708 (2008).
[23] G. J. Nieuwenhuys, Phys. Rev. B **35**, 5260 (1987).
[24] H. Amitsuka, T. Sakakibara, K. Sugiyama, T. Ikeda, Y. Miyako, M. Date, and A. Yamagishi, Phys. B (Amsterdam, Neth.) **177**, 173 (1992).
[25] D. Schulze Grachtrup, M. Bleckmann, B. Willenberg, S. Süllow, M. Bartkowiak, Y. Skourski, H. Rakoto, I. Sheikin, and J. A. Mydosh, Phys. Rev. B **85**, 054410 (2012).
[26] D. Schulze Grachtrup, M. Bleckmann, S. Süllow, B. Willenberg, H. Rakoto, Y. Skourski, and J. A. Mydosh, J. Low Temp. Phys. **159**, 147 (2010).
[27] S. Elgazzar, J. Rusz, P. M. Oppeneer, and J. A. Mydosh, Phys. Rev. B **86**, 075104 (2012).
[28] G. Zwicknagl, Rep. Prog. Phys. **79**, 124501 (2016).
[29] M. Bleckmann, A. Otop, S. Süllow, R. Feyerherm, J. Klenke, A. Loose, R. W. A. Hendrikx, J. A. Mydosh, and H. Amitsuka, J. Magn. Magn. Mater. **322**, 2447 (2010).
[30] R. Daou, F. Weickert, M. Nicklas, F. Steglich, A. Haase, and M. Doerr, Rev. Sci. Instrum. **81**, 033909 (2010).
[31] M. Jaime, R. Daou, S. A. Crooker, F. Weickert, A. Uchida, A. Feiguin, C. D. Batista, H. A. Dabkowska, and B. D. Gaulin, Proc. Natl. Acad. Sci. USA **109**, 12404 (2012).
[32] Y. S. Oh, K. H. Kim, P. A. Sharma, N. Harrison, H. Amitsuka, and J. A. Mydosh, Phys. Rev. Lett. **98**, 016401 (2007).
[33] O. K. Andersen, Phys. Rev. B **12**, 3060 (1975).
[34] H. L. Skriver, *The LMTO Method*, Springer Series in Solid State Sciences Vol. 41 (Springer, Berlin, 1984).
[35] N. E. Christensen, Int. J. Quantum Chem. **25**, 233 (1984).
[36] R. C. Albers, A. M. Boring, and N. E. Christensen, Phys. Rev. B **33**, 8116 (1986).
[37] U. von Barth and L. Hedin, J. Phys. C **5**, 1629 (1972).
[38] O. Jepsen and O. K. Anderson, Solid State Commun. **9**, 1763 (1971).
[39] G. Lehmann and M. Taut, Phys. Status Solidi B **54**, 469 (1972).
[40] J. A. Mydosh and P. M. Oppeneer, Rev. Mod. Phys. **83**, 1301 (2011).
[41] G. W. Scheerer, W. Knafo, D. Aoki, G. Ballon, A. Mari, D. Vignolles, and J. Flouquet, Phys. Rev. B **85**, 094402 (2012).